Soft Failure Localization during Commissioning Testing and Lightpath Operation [Invited]

A. P. Vela, B. Shariati, M. Ruiz, F. Cugini, A. Castro, H. Lu, R. Proietti, J. Comellas, P. Castoldi, S. J. B. Yoo, and L. Velasco

***Abstract*—In Elastic Optical Networks (EONs), effective soft failure localization is of paramount importance to early detect service level agreement (SLA) violations while anticipating possible hard failure events. So far, failure localization techniques have been proposed and deployed mainly for hard failures, while significant work is still required to provide effective and automated solutions for soft failures, both during commissioning testing and in-operation phases. In this paper, we focus on soft failure localization in EONs by proposing two techniques for active monitoring during commissioning testing and for passive in-operation monitoring. The techniques rely on specifically designed low-cost optical testing channel (OTC) modules and on the widespread deployment of cost-effective optical spectrum analyzer (OSA). The retrieved optical parameters are elaborated by machine learning-based algorithms running in the agent's node and in the network controller. In particular, the Testing optIcal Switching at connection SetUp timE (TISSUE) algorithm is proposed to localize soft failures by elaborating the estimated BER values provided by the OTC module. In addition, the FailurE causE Localization for optIcal NetworkinG (FEELING) algorithm is proposed to localize failures affecting a lightpath using OSAs. Extensive simulation results are presented, showing the effectiveness of the TISSUE algorithm to properly exploit OTC information to assess BER performance of QPSK-modulated signals and the high accuracy of the FEELING algorithm correctly detecting soft failures as laser drift, filter shift, and tight filtering.**

***Index Terms*—Soft Failure Localization, Active and Passive Optical Monitoring, Elastic Optical Networks.**

I. Introduction

FAILURE localization is a very useful technique since it helps to reduce failure repair times greatly. When a hard failure occurs at the optical layer, the affected traffic needs to be immediately restored using currently available resources [2]-[8]. Nonetheless, some hard failures start as soft failures, and they can be detected as incipient degradations. Therefore, it would be desirable to anticipate and resolve hard failures in order to plan proper actions like traffic rerouting. Even though some soft failures evolution might take a long time, they can affect the quality of optical connections (*lightpaths*) while in operation.

Manuscript received July 1st, 2017. This work extends the one presented at OFC [1].

Alba P. Vela, Behnam Shariati, Marc Ruiz, Jaume Comellas, and Luis Velasco (lvelasco@ac.upc.edu) are with the Optical Communications Group (GCO) at Universitat Politècnica de Catalunya (UPC), Barcelona, Spain. Filippo Cugini is with CNIT, Pisa, Italy. Alberto Castro, Hongbo Lu, Roberto Proietti, S. J. Ben Yoo are with the University of California (UC Davis), Davis, California, USA. Piero Castoldi is with Scuola Superiore Sant'Anna, Pisa, Italy.

In addition, to guarantee that the resources supporting a lightpath (optical switching and amplification) perform properly before it can enter into operation thus avoiding service level agreement (SLA) violations, telecom operators test its performance by injecting a *test signal* in the ingress node and measuring the bit error rate (BER) in the egress node (commissioning testing). However, optical connection commissioning tests usually need human intervention, where typically two technicians with test equipment travel and stay in front of the end nodes to carry out the end-to-end tests. In addition, if high BER is measured at the egress node, more testing in intermediate nodes need to be performed to localize its cause.

Several works can be found in the literature for *hard* failure localization in optical networks. For instance, authors in [9] proposed a monitoring trail (m-trail) mechanism for fast link failure localization as a result of a fiber cut. Based on defining different monitoring cycles and analyzing a set of alarm signals generated in each monitor of the cycle, failure localization is achieved. Authors in [10] presented a failure location algorithm to locate single and multiple failures in transparent optical networks by analyzing the received alarms. Regarding *soft* failures, vendors have lately commercialized products to track lightpaths along their route [11] or to predict network health [12].

Note that any of the above techniques allow the identification of *soft* failures affecting individual lightpaths, such as laser drift, filter shift, or tight filtering, and thus in-line monitoring techniques to analyze and evaluate the quality of individual optical lightpaths are required. In this regard, although Optical Spectrum Analyzers (OSA) could be used to analyze the spectrum of optical signals, until recently, the use of OSA in the network was very limited due to the high cost of accurate OSAs. However, improvements in OSA technology are taking place, and a new generation of cost-effective OSAs with sub-GHz resolution is now available to be integrated into a new generation of optical nodes [13]. Furthermore, OSA and other monitoring techniques require sophisticated algorithms able to identify and localize failures. These algorithms can be deployed in the network controller, as well as in nodes' agents, close to the monitoring points, to reduce the amount of monitoring data to be conveyed to the control/management plane [14].

In our previous work [1], [15], we focused on detecting in advance excessive BER in lightpaths and proposed the BER Anomaly Detection (BANDO) algorithm. Once a BER

degradation is detected, it is of paramount importance to identify and localize the failure, e.g. for in-operation network reconfiguration [16].

Notwithstanding the availability of OSA monitoring systems in the optical nodes, their use assumes the existence of an optical signal to be analyzed, something that might not be true in some situations, such as during lightpaths' commissioning testing.

To reduce human intervention, active monitoring techniques were developed in the context of IP networks; they generally consist in generating and injecting a test signal that is used to measure metrics across Internet paths [17]. Although no similar active monitoring techniques are available at the optical layer, lightpath monitoring techniques have been previously studied. Specifically, the authors in [18] introduced the optical supervisory channel (OSC) technique to monitor the BER of a lightpath (single carrier or superchannel) in different points along its route by using low-speed (few hundreds of MHz) electro-optical components. The OSC technique consists in over-modulating the lightpath to be monitored with a low modulation index and low-speed On-Off Keying (OOK) signal; it allows to estimate the BER of the high-speed phase modulated signal (e.g., 100 Gb/s Dual Polarization - Quadrature Phase Shift Keying (DP-QPSK)) with sufficient accuracy by BER correlation curves calculated a priori. We propose to apply a similar concept for commissioning testing and failure localization purposes; we name it as optical testing channel (OTC). The main difference is that, in OTC, the low-speed low-index OOK modulation is applied to a continuous-wave laser rather than to a high-speed coherent signal. The modulation parameters in OTC are the same as in OSC to guarantee accurate BER estimation while requiring simple and low-cost hardware for the operator.

In this paper, we focus on soft failure localization in Elastic Optical Networks (EON) during commissioning testing and once lightpaths are in operation. In the rest of the paper, unless explicitly stated otherwise, we just use failure localization for the sake of brevity. We propose the OTC for active monitoring during commissioning testing, as well as the use of OSAs for passive monitoring. Both monitoring systems are based on a hierarchical architecture to support local and centralized data analytics, where optical nodes and network controller are extended with local and global data analytics capabilities, respectively (see [19] and [20]). The techniques presented in this paper highly depend on the modulation format of the lightpaths, so we restrict ourselves to focus specifically on QPSK-modulated signals since it is the most common modulation format used in medium and long reach telecom operator networks. Specifically, the contribution of this paper is three-fold:

- Section II presents our proposals for BER estimation and failure localization during the commissioning phase and failure localization based on OSAs triggered by the detection of excessive BER in a lightpath once it is in operation. A node architecture equipped with OSAs and OTC modules is proposed and modules running in the agent's node and in the network controller are presented.
- Section III focuses on designing the OTC system to be used during commissioning testing. System designs of the transmitter and receiver modules are detailed. Besides, the Testing optIcal Switching at connection SetUp timE (TISSUE) algorithm that received estimated BER and localizes failures is presented.
- Section IV targets at localizing failures affecting a lightpath using OSAs. A number of features are proposed to characterize the spectrum of a DP-QPSK signal. Those features are exploited by machine learning-based algorithms to detect degradations and identify failure classes. The FailurE causE Localization for optIcal NetworkinG (FEELING) algorithm running in the network controller uses these modules to localize, classify and estimate the magnitude of the failure.

The discussion is supported by the results from simulation presented in Section V.

II. Before and In-operation Failure Localization

Two different scenarios for failure localization can be defined: *i*) during customer lightpaths' commissioning testing to ensure the proper lightpath performance before they are delivered and enter into operation. Note that since excessive BER might lead to SLA violations, BER needs to be checked at the reception side and, in the case of excessive BER, the source of the errors should be localized as accurately as possible. At this point, we assume that transponders are at the customer side and that the lightpath is already established in the network between ingress and egress nodes at the switching level, so active monitoring can be applied by injecting a *test signal*; and *ii*) once a lightpath is in operation, BER can be measured, and BER degradations can be detected in advance before reaching excessive BER levels [1], [15]. Once detected, the cause of failure needs to be localized, this time by using passive monitoring techniques, to facilitate lightpath rerouting.

For these scenarios, we propose the use of two monitoring systems to be installed in the optical network nodes: a redesigned OSC and OSAs. Here, the concept of OSC is redefined and renamed as OTC, where the OTC_{Tx} module is equipped with a tunable laser and a pseudo-random bit sequence (PRBS) generator to create a test signal. Then, the OTC_{Rx} receives the test signal and estimates the BER (see the details of this new OTC in Section III).

Fig. 1 presents a very simplified diagram of the architecture of an optical node, where only one incoming and one outgoing links, as well as the local signals being dropped and added are represented. The node consists of wavelength-selective-switches (WSS), optical amplifiers (OA), dispersion compensation fiber (DCF) and channel equalizers; on the architecture, OTC and OSA monitoring systems are highlighted. OTC modules are connected to local WSS in the architecture in Fig. 1. Since OTC modules use low-speed

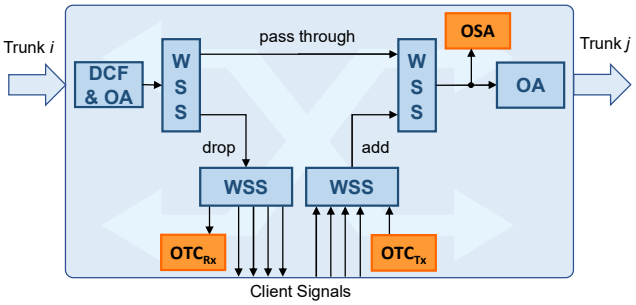

Fig. 1. Simplified optical node architecture with OTC and OSA monitoring systems

electronics, its expected cost is very small. In addition, only one single OTC_{Tx} and one single OTC_{Rx} modules per node need to be equipped, which although limits the number of concurrent test that can be carried out, also limits the number of consumed local WSS ports, which has a significant impact on the cost of the ROADMs [21]. On the other hand, OSAs are placed in every outgoing link, so the number of OSAs per node equals to the nodal degree. In this case, we have limited the number of OSAs due to its cost, and although failure localization can still be carried out, the granularity of the localization would be at the node level. To achieve a finer failure location granularity, more OSAs should be placed, consequently increasing the node cost.

Fig. 2 shows an example of the use of the proposed OTC monitoring system for before-operation tests and failure localization. One OTC_{Tx} is used in the ingress node to generate the test signal, and one OTC_{Rx} per intermediate and egress node is used to estimate the BER. Note that, since the lightpath has not been delivered to the customer yet, the client signal is not connected to the lightpath neither in the ingress nor the egress node at this stage. A module named as Signal Quality Estimation (SQE) running in the node's agent is in charge of receiving the measured BER in the local OTC and correlate to what the client signal would observe. The TISSUE algorithm, running in the network controller, is in charge of allocating the OTC modules in the network nodes, setting-up the local connections from them to the lightpath in the end nodes, receiving BER estimations and deciding whether the tests pass or not, and estimating the elements that participate in the excessive BER.

Fig. 3 depicts the use of OSAs to localize soft failures once the lightpath is in operation. OSAs acquire the whole C-band spectrum, and then, data for the portion of the spectrum allocated to the lightpath under study is extracted. OSAs passive monitoring is carried out in the ingress and every intermediate node (but not in the egress one). Two modules running in node's agent are in charge of analyzing the spectrum: *i*) the Feature Extraction (FeX) module first finds the set of relevant points in the signal spectrum that are used to compute meaningful signal features; and *ii*) the Signal Spectrum Verification (SSV) module that targets at analyzing the extracted features to detect misconfigurations, i.e., central frequency drift and filtering problems.

The FEELING algorithm, running in the network controller, is in charge of commanding the modules in the nodes and to receive a diagnosis, as well as the relevant signal points from them to localize the failure and estimate its magnitude. It is worth mentioning that FEELING must be able to distinguish between actual failures and normal effects that could lead to similar evidence, specifically tight filtering effects due to filter cascading of a normal signal. FEELING takes advantage of the Signal Spectrum Comparison (SSC) module that generates a diagnosis of one signal focusing specifically on filtering problems. In addition, failure magnitude estimation modules (Laser Drift Estimator, Filter Shift Estimator (FSE), and Filter Tightening Estimator (FTE)) quantify specific failure effects.

The next two sections are focused on the design of the proposed active and passive monitoring systems.

III. Use Case I: Commissioning Tests and Failure Localization

Fig. 4 shows the OTC system design, where a continuous-wave laser is OOK modulated by a Mach-Zehnder (MZ) modulator. A PRBS pattern generator implementable with a low-cost FPGA drives the modulator directly (no RF amplifier is required since the modulation speed is below 1 GHz with low modulation index). At different intermediate nodes, the OTC channel is dropped and received with a simple low-bandwidth photoreceiver (detector plus trans-impedance amplifier) connected to a BER tester (this can also be implemented in an FPGA).

Note that, it is necessary for the operator to linearly adjust the modulation speed of the OTC channel according to the baud-rate of the lightpath requested by the client. Therefore, the bandwidth of the OTC system components should be large enough to account for the highest possible lightpath baud rate. However, this is not a critical aspect since the OTC modulation speed can usually be hundreds time slower than the client signal. In this section, we assume 25 GBd DP-QPSK client signals and OTC is 250Mb/s OOK. A BER conversion model (e.g., table or function) translates the OTC measured BER value into a client QPSK signal estimated BER (see Section V).

As introduced above, the TISSUE algorithm running in the network controller is in charge of collecting the QPSK signal estimated BER from each of the intermediate nodes; the SQE module is in charge of acquiring the OTC BER and use the BER conversion model to obtain the estimated BER.

Initially, TISSUE algorithm (Table I) allocates the OTC modules in the network nodes along the route of the lightpath and sets up the needed connections between the OTC modules and the lightpath so the OTC_{TX} module injects the test signal in the ingress node and all the OTC_{RX} modules get the test signal to measure BER (lines 1-2 in Table I). Next, the QPSK BER estimated values are collected from the SQE modules, and theoretical BER values are computed based on OSNR values [22] (lines 3-5).

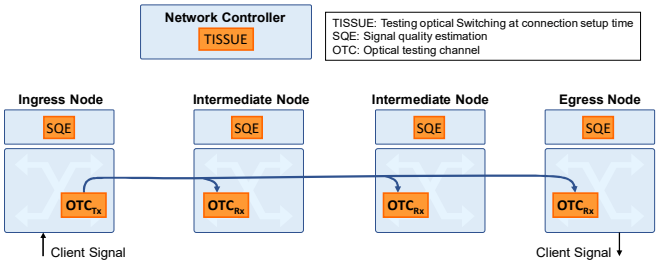

Fig. 2. OTC active monitoring for commissioning testing and failure localization

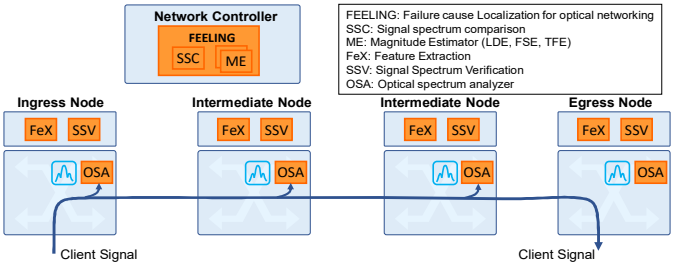

Fig. 3. OSA passive monitoring for in-operation failure localization

TABLE I TISSUE ALGORITHM

INPUT *lightpath*
OUTPUT *FailureList*

1: <otc_{Tx}, OTC_{Rx}> ← allocateResources (*lightpath*)
2: setupConnections (*lightpath*, {otc_{Tx}} ∪ OTC_{Rx})
3: **for each** $r \in OTC_{Rx}$ **do**:
4: BER.estim[r] ← getEstimatedBER(r)
5: BER.theo[r] ← computeTheoBER(*r.node, lightpath*)
6: failures ←∅
7: **for** i = 1..|OTC_{Rx}|-1 **do:**
8: *estimSlope* ← compSlope(*BER.estim*[i],*BER.estim*[i+1])
9: *theoSlope* ← compSlope(*BER.theo*[i], *BER.theo*[i+1])
10: **if** *estimSlope / theoSlope* > α **then**
11: *failures* ←*failures* ∪ {<i, i+1>}
12: deAllocateResources (*lightpath*, otc_{Tx}, OTC_{Rx})
13: **return** *failures*

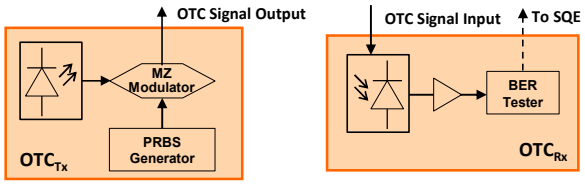

Fig. 4. OTC system design: a) OTC transmitter and b) OTC receiver

Finally, we compute the difference between the slopes of both estimated and theoretical BER in each span to determine the existence of a failure; if the slopes difference is above a maximum value, a failure has been detected in such span (lines 6-11). The OTC modules are released (line 12) and the list of spans in failure is eventually returned (line 13).

IV. USE CASE II: IN-OPERATION FAILURE LOCALIZATION

In this section, we focus on the use of OSAs to localize failures once the lightpath is in operation. Fig. 5a shows an example of 100Gb/s DP-QPSK modulated optical spectrum acquired by an OSA with 625 MHz granularity. In general, QPSK optical signals present a flat spectral region around the central frequency, sharp edges, and a round region between the edges and the central frequency. When the signal is properly configured, its central frequency should be around the center of the assigned spectrum slot to avoid filtering effects, and it should be symmetrical with respect to its central frequency. On the contrary, in the case of laser drift, the central frequency of the signal would be shifted with respect to the assigned slot, it would be asymmetrical in the case of filter shift, and the edges get noticeably rounded in the case of tight filtering.

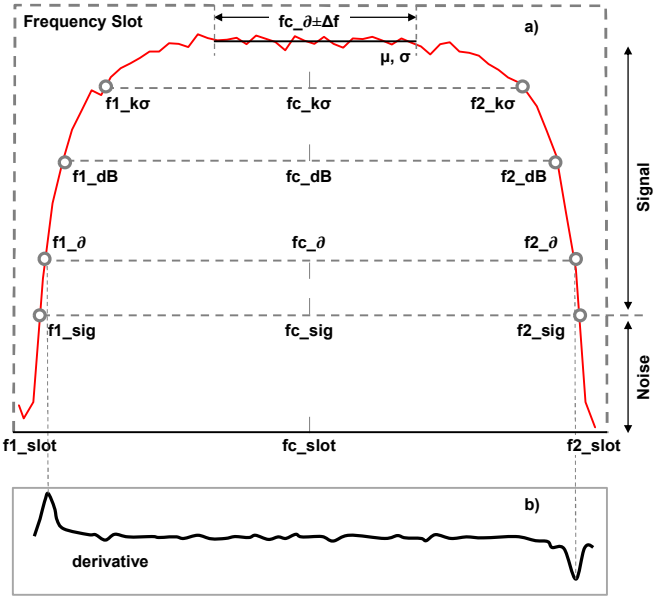

Fig. 5. Relevant signal points (primary features)

In order to detect the above distortions, the FeX module primarily pre-processes the optical spectrum of the signal, which formally consists of an ordered list of frequency-power (<f, p>) pairs. The first pre-processing step consists in equalizing power, so the maximum power to be 0 dBm. Then, the derivative of the power with respect to the frequency is computed. Fig. 5b illustrates the derivative of the example optical signal; note that sharp convexity is observed close to the edges.

After pre-processing, the FeX module characterizes the mean (μ) and the standard deviation (σ) of the power around the central frequency ($fc\pm\Delta f$), as well as a set of primary features computed as cut-off points of the signal with the following power levels: *i*) equalized noise level, denoted as *sig* (e.g., -60dB + equalization level); *ii*) edges of the signal computed using the derivative, denoted as ∂; *iii*) a family of power levels computed with respect to μ minus $k\sigma$, denoted as $k\sigma$; and *iv*) a family of power levels computed with respect to μ minus a number of dB, denoted as *dB*. Each of these power levels generates a couple of cut-off points denoted as $f1_{(\cdot)}$ and $f2_{(\cdot)}$. In addition, the assigned frequency slot is denoted as $f1_{\text{slot}}$, $f2_{\text{slot}}$. These features (hereafter denoted as X), are used as input for class identification and magnitude estimation modules trained using features from reference signals.

Although features have been computed from an equalized signal, note that signal distortion due to filter cascading effect has not been corrected yet. As previously introduced, this effect might induce to a wrong diagnosis of a filter problem for a normal signal. To overcome this drawback, we use a *filter mask* to compensate the effect that a normal signal would suffer after passing a defined number of filters before computing its features. Filter masks can be easily obtained by means of the theoretical signal filtering effects or experimental measurements taken for a distinct number of cascaded filters. Every time FEELING asks for diagnosis at a given intermediate node of a lightpath, it sends the specific filter mask to the node to correct the features.

Other features are computed as linear combinations of the primary features focus on characterizing a given optical signal; they include: *i*) bandwidth, computed as $bw_{(\cdot)}=f2_{(\cdot)}-f1_{(\cdot)}$; *ii*) central frequency, computed as $fc_{(\cdot)}=f1_{(\cdot)}+0.5*bw_{(\cdot)}$, as well as the shifting of the central frequency $\Delta fc_{(\cdot)}=fc_{(\cdot)}-fc_{(\text{slot})}$; and *iii*) symmetry with respect to a reference (frequency slot or derivatives), computed as $sym_{(\cdot)\text{-ref}}=(f1_{(\cdot)}-f1_{\text{ref}})-(f2_{\text{ref}}-f2_{(\cdot)})$.

Once the FeX module computes the features of the signal, the SSV module uses them to generate a diagnosis, which consists of: *i*) a predicted class among the following options: '*Normal'*, '*LaserDrift'*, '*FilterFailure'*; and *ii*) a subset of signal features ($X' \subseteq X$) for the predicted class. SSV module includes thus a multiclass classifier in the form of a decision tree that receives as input a set of features for a signal and returns the predicted class. Basically, the decision tree contains a number of *decision rules* to map specific combinations of feature values to classes. Each decision rule is a sequence of binary tests starting from the root node to a leaf node that characterizes one and only one class.

Decision trees are easily generated (trained) from a training dataset containing labeled samples (sets of features and their class) [23]. Notwithstanding, to avoid overfitting, trees need to be limited in size in terms of number of decision rules without significantly sacrificing accuracy. An approach to limit tree size is to force the minimum number of samples that are in a leaf node. Table II illustrates the proposed algorithm to that end; it receives a dataset that is firstly balanced by replicating samples for the less frequent classes, and it is then randomly split into training and testing (lines 1-2 in Table II).

After few initializations (lines 3-5), an iterative procedure is executed to fit a tree with a minimum number *n* of samples per leaf between *nmin* and *nmax*. For every *n*, a decision tree is fitted from the training dataset and the error, defined as wrong classified samples over the total number of samples is computed for both training and testing datasets (lines 6-9). The best number of samples (*N*) is updated if error from testing dataset has been reduced (lines 10-13) or, in case obtaining the minimum error obtained so far, the difference between error from training and from testing is reduced (lines 14-18). The tree fitted with the input dataset and *N* is eventually returned (line 19).

TABLE II SSV TREE GENERATION ALGORITHM

INPUT *dataset, nmin, nmax*
OUTPUT *tree*

```
1:  dataset←balanceClassesByReplication(dataset)
2:  <training,testing>←randomSplit(dataset)
3:  N←Ø
4:  minDiff←∞
5:  minError←∞
6:  for n=nmin..nmax do
7:      tree ← fitTree(training, n)
8:      errorTesting ←predict(tree, testing)
9:      errorTraining ←predict(tree, training)
10:     if errorTesting<minError then
11:         N←n
12:         minError←errorTesting
13:         minDiff←|errorTraining-errorTesting|
14:     else if errorTesting=minError then
15:         diff←|errorTraining-errorTesting|
16:         if diff≤minDiff then
17:             N←n
18:             minDiff←diff
19: return fitTree(dataset, N)
```

TABLE III FEELING ALGORITHM

INPUT *lightpath*
OUTPUT {<*node, class, magnitude*>}

```
1:  ingress ← lightpath.getNodeFromRoute (1)
2:  lastInterm ← lightpath.getNodeFromRoute (-2)
3:  FM ← getFilterMasks(lightpath)
4:  diagIngress ← getFailureDiagnosis (ingress, FM (1))
5:  diagLast ← getFailureDiagnosis (lastInterm, FM (-2))
6:  if diagIngress.class = diagLast.class AND
                diagIngress.class = Normal then
7:      return {<1, Normal, ->}
8:  if diagIngress.class =LaserDrift then
9:      magn← LDE(diagIngress.X)
10:     return <1, LaserDrift, magn>
11: XNodeChange ← diagIngress.X
12: diagChange = <class, magn> ←SSC (diagIngress.X)
13: if diagChange.class<> normal then
14:     FailureSet←<1, diagChange>
15: else FailureSet ← ∅
16: for i=2..lightpath.RouteLength()-1 do
17:     node_i ← lightpath.getNodeFromRoute (i)
18:     Xi← getSignalPoints (node_i)
19:     diagNode_i ← SSC (Xi)
20:     if diagNode_i.class <> diagNodeChange.class OR
            diagNode_i.magn - diagNodeChange.magn > α then
21:         XNodeChange ← Xi
22:         FailureSet ← FailureSet ∪ {<i, diagNode>}
23: return FailureSet
```

Similarly as the SSV module, the SSC module generates a diagnosis of one signal focusing specifically on filtering problems; it classifies signals into three classes: *Normal*, *FilterShift*, *TightFiltering*. SSC consists of a hierarchy of two binary classifiers: the first one predicts whether the captured optical spectrum is *Normal* or has suffered from filter-related failure. In the case of predicting a failure, a second binary classifier is used to predict whether the failure is due to *FilterShift* or *TightFiltering*.

The decision-making units of SSC module are realized as supervised support vector machine (SVM) binary classifiers exploiting i^{th} order polynomials as kernel function [24]. In

order to obtain an SVM model, a similar approach to the one for the decision tree in the SSV module was followed, where the loop is iterated on both, the cost of misclassifying and the degree of the polynomial kernel, which are parameters to control the complexity and size of the SVM. The SVM generation algorithm returns the SVM with the optimal parameter configuration.

When a filter related failure is detected, either a Filter Shift Estimator (FSE) or a Filter Tightening Estimator (FTE) is called to estimate the magnitude of the failure as a function of few selected features; linear regression for the magnitude estimators was used since both, magnitudes and features take real values. In order to find the proper set of features, we apply a stepwise approach that aims at finding the model with the optimum balance between accuracy and number of coefficients (i.e., features) in terms of the Akaike Information Criterion (AIC) [24].

Finally, the FEELING algorithm that uses the above-defined modules is detailed in Table III; recall that FEELING is called upon the detection of excessive BER at the reception side of an optical signal. The algorithm first calls FeX and SSV modules in the ingress and last intermediate extended nodes to perform signal verification and obtain a diagnosis (lines 1-5 in Table III). In the case that the diagnosis of both nodes is normal, FEELING ends with no failure detected (lines 6-7). Otherwise, in the event of laser drift diagnosis at the ingress, the Laser Drift Estimator (LDE) module is run to measure failure magnitude (lines 8-10); for LDE modeling, we considered linear regression.

In the case of a different diagnosis, FEELING starts a procedure to detect filter related problems at intermediate nodes using the SSC module to compare diagnosis and magnitudes between nodes in the route of the lightpath. This process starts with the diagnosis at the ingress node that it is used as the initial reference node (lines 11-14). Then, the diagnosis of every intermediate node is compared against the one of the reference changing node and failure set is updated if either a new filter failure is detected or the magnitude increased above a certain threshold (lines 15-22). After processing all intermediate nodes, the list of failures detected is eventually returned (line 23).

V. Results

This section reports the obtained results from simulating scenarios for commissioning testing and in-operation failure localization.

A. Optical Testing Channel.

Regarding commissioning testing, we performed Monte Carlo simulations with a 250Mb/s OOK channel transmission with the OTC scheme described in Section III. In the simulation, the signal propagates through 1000km of single mode fiber, which consists of ten 100km-spans, a set of DCF to mitigate the chromatic dispersion effect, and a set of EDFA amplifiers. The fiber attenuation coefficient is 0.2dB/km, the noise figure of EDFAs is 4dB, and the fiber nonlinear coefficient is 1.37 $(W\ Km)^{-1}$.

The fiber propagation is simulated using the split-step method, with a step size of 0.1 km. To maintain the BER lower than 3.7×10^{-3} at 1000 km (7% FEC threshold), the launched power is set to -17dBm. In the OTC_{RX}, the low-speed photo detector has 1GHz bandwidth. We assume that amplified spontaneous emission (ASE) noise dominates the noise spectrum and other noises or distortions are negligible. Finally, after several tests, we set TISSUES's parameter α to 2.

To study the correlation between OTC measured BER and QPSK signal estimated BER, we simulated the OTC scheme, as well as 25GBd QPSK signal and measured the BER after every span; Fig. 6a plots the obtained BER relation. It can be shown that there is an almost near linear relationship between the BER of the OTC channel at 250Mb/s and the BER of a QPSK channel. Note that the above BER relation is specific for the particular case where the signal does not traverse any filter. Because the signal will be affected by intermediate filters, different OTC vs. QPSK BER correlation curves need to be used as a function of the number of filters that the signal has traversed. Then, family of piece-wise linear models can be used to convert the measured OTC BER to the estimated QPSK signal BER as a function of the number of filters. Such models are stored in every SQE module and used every time the TISSUE algorithm requests BER estimation.

At lightpath commissioning testing, the TISSUE algorithm requests SQE modules along the route of the lightpath to obtain BER estimations and compares them against theoretically computed values. Fig. 6b plots an example of theoretical and estimated BER for the last seven 100km spans of the simulated 10-span scenario (the first three spans are not shown since their BER is lower than 10^{-7}). As observed, values are very close (about half decade difference in BER values), proving that the OTC scheme is an effective testing technique for operators to check the quality of a new lightpath, as well as to localize spans with excessive BER.

Finally, to evaluate the TISSUE algorithm, we added 2dB of noise after span #5. Fig. 6c plots the estimated QPSK BER and the theoretical BER for the last seven spans. TISSUE localizes the failure after noticing the large estimated BER slope compared to the theoretical one.

B. Optical Spectrum Analyzer.

Regarding in-operation failure localization, we set up the scenario in VPIPhotonics illustrated in Fig. 7. In the transmitter side, a 30 GBd DP-QPSK signal is generated (120 Gb/s lightpath). The signal passes through 10 single mode fiber spans. After each span, an optical amplifier compensates for the accumulated attenuation of the fiber. Each node is modeled as a single optical filter with a 2nd order Gaussian transfer function emulating optical switching functionality performed by several WSSs; filters bandwidth is set to 37.5 GHz, leaving 7.5 GHz as a guard band for the lightpath.

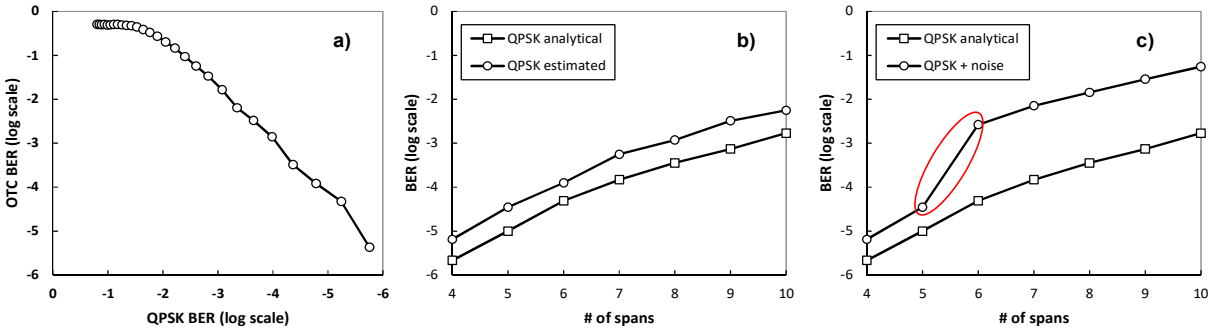

Fig. 6. a) OTC vs. 25GBd QPSK BER correlation. b) Estimated QPSK BER vs. theoretical QPSK BER. c) Degraded BER and failure localization.

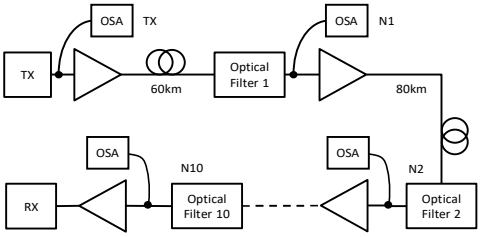

Fig. 7. VPI setup

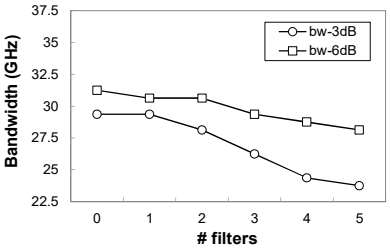

Fig. 8. Impact of filter cascading

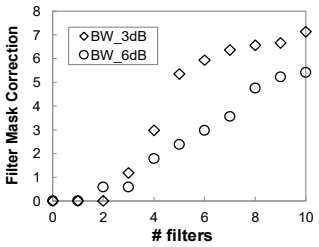

Fig. 9. Filter masks for two features

Finally, the DP-QPSK signal ends in a coherent receiver that compensates for the impairments introduced throughout the transmission. Emulating the optical node architecture in Fig. 1, coarse-granular OSAs are placed after every filter to analyze the optical spectrum. OSAs have been configured with a granularity of 625 MHz, i.e., every 37.5 GHz frequency slot is represented by 60 <f, p> pairs.

Simulations have been carried out to produce a database of samples belonging to different failure classes (including normal operation): *i*) for *LaserDrift* failures, a frequency shift is applied to the laser emission frequency; the frequency of the local oscillator at the Rx side is configured accordingly; *ii*) for *FilterShift* failures, a frequency shift is applied to the central frequency of filters; *iii*) *TightFiltering* failures are emulated by modifying the bandwidth of the filter. Regarding failure magnitudes, although we simulated a wide range of them, we considered as actual failures those with a magnitude higher than a certain threshold, while samples below the threshold were re-labeled as normal. Specifically, thresholds were set to 1.5GHz for *LaserDrift*, 3 GHz for *FilterShift*, and 32 GHz for *TightFiltering*. Recall that *TightFiltering* magnitude increases when filter bandwidth decreases.

It is worth mentioning that the *TightFiltering* failure needs to be distinguished from filter cascading. Fig. 8 shows the evolution of features $bw_{\text{-3dB}}$ and $bw_{\text{-6dB}}$ for a DP-QPSK signal in terms of the number of filters that the signal passes through when all the components operate properly. As shown, bandwidth constantly decreases after the 2nd filter, which anticipates the difficulty to correctly distinguish between the *Normal* class and *TightFiltering* failure in some scenarios.

In view of the above, the training of classifier and magnitude prediction modules has been carried out with a shorter testbed (only two spans and filters between Tx and Rx) to avoid mispredicting filter cascading as filter failure. 28 distinct configurations of failure and magnitude have been simulated, generating up to 500 different samples for training and testing. Each sample consists of 56 different features obtained at several power levels.

Let us first focus on SSV tree generation. Recall that SSV classifies among three classes: *Normal*, *LaserDrift*, and *FilterFailure*. After executing the algorithm in Table II, the optimal tree (with N=15) consists of three leaf nodes, each characterized by a decision rule that depends on five features: bw_{∂}, $bw_{\text{-3dB}}$, $bw_{\text{-6dB}}$, $sym_{\text{-3dB-}\partial}$, and $sym_{\text{-6dB-}\partial}$. Average and maximum classification errors (in terms of the proportion of wrong decisions) were 3% and 9%, respectively. Both *Normal* and *LaserDrift* classes are always well predicted, whereas 9% of *FilterFailure* problems are classified as *LaserDrift*. In light of these results, we can conclude that SSV provides accurate failure detection and identification.

Classifiers in the SSC module are based on the same features used by SSV. The first classifier, which is in charge of identifying between normal and filter failures, provides no classification error. This result is the key for the failure localization process since we can conclude that SSC provides perfect localization of a failed filter in the absence of filter cascading effects. The second classifier, used upon the localization of a failure to distinguish between *FilterShift* and *TightFiltering*, returns a classification error around 18%. Although this error is not negligible, it is worth noting that its negative impact is small since filter failure identification is not as crucial as filter failure localization. Finally, magnitude predictors were fitted with different combinations of the above-mentioned features (LDE: Δfc_{∂}, FSE: Δfc_{∂} and $sym_{\text{-3dB-slot}}$, and FTE: $bw_{\text{-3dB}}$) to provide highly accurate linear models with average errors below 5%.

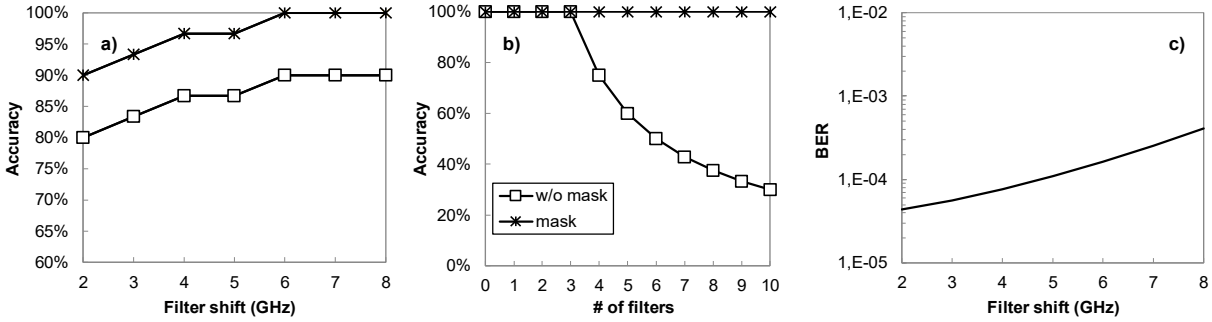

Fig. 10. FEELING performance for *FilterShift* failure localization

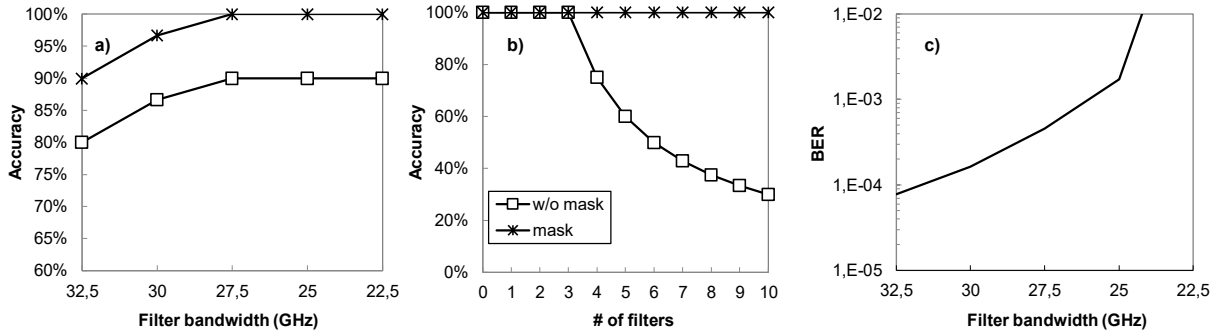

Fig. 11. FEELING performance for *TightFiltering* failure localization

Once classifiers and predictors have been successfully trained and validated, let us evaluate the performance of FEELING in the setup of Fig. 7. The behavior of filter bandwidth degradation due to filter cascading shown in Fig. 8 has been used to set up the filter mask applied to every intermediate node before running failure diagnosis (Fig. 9 shows filter mask additive corrections as a function of the number of filters for bw_{-3dB}, bw_{-6dB} features). As for previous results, we carried out simulations for all failures and several magnitudes, considering only one failure per simulation.

For the case of *LaserDrift*, FEELING is able to localize the failure with 100% of accuracy, which is a consequence of the high accuracy of SSV and the fact that in our simulations, the transmitter was collocated with the ingress node, and thus the signal arrives without any filter cascading effects. For the case of filter related failures, Fig. 10 and Fig. 11 illustrate localization accuracy for *FilterShift* and *TightFiltering*, respectively. Accuracy in terms of the proportion of correct localizations is provided as a function of the magnitude of the failure (Fig. 10a and Fig. 11a) for two distinct cases: with and without applying filter mask. The conclusion is that, as soon as the failure magnitude increases, localization accuracy also increases. Additionally, it is seen that the accuracy is higher when the filter mask is used. For *FilterShift* higher than 5GHz and *TightFiltering* smaller than 28 GHz, overall accuracy reaches 100% when filter mask is applied, in contrast to the 90% obtained without filter masks.

Although high enough overall localization accuracy is obtained without filter mask, Fig. 10b and Fig. 11b clearly show the negative effects of filter cascading for failure localization. The figures illustrate the accuracy as a function of the number of cascaded filters before the failure. In the case of filter shift and filter tightening, the values are obtained for magnitudes higher than or equal to 6 GHz and lower than or equal to 27.5 GHz, respectively. As it can be observed, for the case without mask, the localization accuracy decreases sharply when the lightpath passes through more than 3 filters. On the other hand, filter mask correction compensates filter cascading effects and allows 100% of localization accuracy in every of the filters in our setup.

Finally, it is important to recall that FEELING is triggered upon the BANDO algorithm in [1] after detecting excessive BER in the reception of a lightpath. The calibration of BANDO includes BER thresholds that are setup in order to perform prompt and even anticipated BER degradation. Assuming a BER increase due to a gradual degradation of a filter, Fig. 10c and Fig. 11c are provided to illustrate the relation between BER change detection thresholds and failure localization. Those figures depict the simulated BER as a function of failure magnitude. For illustrative purposes, let us imagine that, due to two different configurations, BANDO detects excessive BER at 8E-05 and 5E-04. Without entering into details, the former could correspond to a BER threshold violation anticipation while the latter could represent an actual threshold violation. A BER equal to 8E-05 could correspond to a degraded filter shifted around 4 GHz or narrowed until 32GHz, a failure that is localized with an accuracy around 90%. On the other hand, BER equal to 5E-04 is obtained for failures whose magnitude is large enough to localize them without localization errors. Hence, modules for BER degradation and failure identification and localization must be configured with a global perspective to achieve optimal overall performance.

VI. Concluding Remarks

Proper operation of the network components is a key factor to provide the expected quality of service to the end-users and avoid violating service level agreements (SLA). Therefore, predicting upcoming failures that can disrupt the network operation, by continuous monitoring of the active lightpaths is of great importance. In this paper, we proposed two monitoring systems to intelligently identify and localize failure during commissioning testing and lightpath operation.

In the case of commissioning testing, the low cost and complexity OTC system was proposed and validated as a promising technique for estimating the BER of a 100Gb/s DP-QPSK modulated lightpath. Simulations showed that the OTC the estimated BER can be used for testing and failure localization.

For the case of lightpath operation, a machine-learning based identification and localization platform (called FEELING) was proposed, taking advantage of continuous monitoring of the optical spectrum using cost-effective OSAs installed in the optical nodes. FEELING predicts whether a component is failed and, in the case of failure, estimates the magnitude of the failure. In this work, we focused on three classes of failures: *LaserDrift*, *FilterShift*, *TightFiltering*. In order to evaluate the accuracy of FEELING, we performed an extensive set of simulations, and the results showed that FEELING identifies/localizes *LaserDrift* with 100% of accuracy. In the case of filter related failures, FEELING can identify/localize the failure with the accuracy above 90%.

Acknowledgment

The authors would like to thank Gengchen Liu for his valuable help.

This work was partially supported by the EC through the METRO-HAUL (G.A. nº 761727) project, by the Spanish MINECO SYNERGY project (TEC2014-59995-R), by the Catalan Institution for Research and Advanced Studies (ICREA), and by the DoE under grant DE-SC0016700.

References

[1] A. P. Vela, M. Ruiz, F. Fresi, N. Sambo, F. Cugini, L. Velasco, and P. Castoldi, "Early Pre-FEC BER Degradation Detection to Meet Committed QoS," in Proc. Optical Fiber Communications Conference and Exhibition (OFC), 2017.

[2] F. Paolucci, A. Castro, F. Cugini, L. Velasco, and P. Castoldi, "Multipath Restoration and Bitrate Squeezing in SDN-based Elastic Optical Networks," (Invited Paper) Springer Photonic Network Communications, vol. 28, pp. 45-57, 2014.

[3] Y. Pointurier, "Design of low-margin optical networks," IEEE/OSA Journal of Optical Communications and Networking, vol. 9, pp. A9-A17, 2017.

[4] K. Christodoulopoulos, N. Sambo, E. Varvarigos, "Exploiting network kriging for fault localization," Optical Fiber Communications Conference and Exhibition (OFC), 2016.

[5] U. Kozat, G. Liang, K. Kokten, J. Tapolcai, "On Optimal Topology Verification and Failure Localization for Software Defined Networks," IEEE/ACM Transactions on Networking, vol. 24, pp. 2899-2912, 2016.

[6] N. Ogino, H. Yokota, "Heuristic Computation Method for All-Optical Monitoring Trails Terminated at Specified Nodes," IEEE/OSA Journal of Lightwave Technology, vol. 32, pp. 467-482, 2014.

[7] X. Li, W. Ji, S. Zhang, K. Huang, "Signaling free localization of link and node failures in an optical mesh-tree network," IEEE/OSA Journal of Optical Communications and Networking, vol. 8, pp. 263-271, 2016.

[8] J. Tapolcai, P. Ho, P. Babarczi, L. Ranyai, "On Signaling-Free Failure Dependent Restoration in All-Optical Mesh Networks," IEEE/ACM Transactions on Networking, vol. 22, pp. 1067-1078, 2014.

[9] B. Wu, P. Ho and K. L. Yeung, "Monitoring Trail: On Fast Link Failure Localization in All-Optical WDM Mesh Networks," IEEE/OSA Journal of Lightwave Technology, vol. 27, pp. 4175-4185, 2009.

[10] C. Mas, I. Tomkos, and O. Tonguz, "Failure Location Algorithm for Transparent Optical Networks," IEEE Journal on Selected Areas in Communications, vol. 23, pp. 1508-1519. 2005.

[11] Nokia. Bringing wavelength agility and efficiency to software-defined networks, [On-line] www.nokia.com, 2016.

[12] Blue Planet Analytics, [On-line] www. blueplanet.com, 2017.

[13] Finisar. Flexgrid High Resolution Optical Channel Monitor (OCM) [On-line] www.finisar.com, 2017.

[14] A. P. Vela, M. Ruiz, L. Velasco, "Distributing Data Analytics for Efficient Multiple Traffic Anomalies Detection," Elsevier Computer Communications, vol. 107, pp. 1-12, 2017.

[15] A. P. Vela, M. Ruiz, F. Fresi, N. Sambo, F. Cugini, G. Meloni, L. Potì, L. Velasco, and P. Castoldi, "BER Degradation Detection and Failure Identification in Elastic Optical Networks," IEEE/OSA Journal of Lightwave Technology (JLT), 2017 (DOI: 10.1109/JLT.2017.2747223).

[16] L. Velasco, A. P. Vela, F. Morales, and M. Ruiz, "Designing, Operating and Re-Optimizing Elastic Optical Networks," (Invited Tutorial) IEEE/OSA Journal of Lightwave Technology (JLT), vol. 35, pp. 513-526, 2017.

[17] S. Shalunov, B. Teitelbaum, A. Karp, J. Boote, M. Zekauskas, "A One-way Active Measurement Protocol (OWAMP)," IETF RFC 4656, 2006.

[18] D. J. Geisler, R. Proietti, Y. Yin, R. P. Scott, X. Cai, N. K. Fontaine, L. Paraschis, O. Gerstel, and S. J. B. Yoo, "Experimental demonstration of flexible bandwidth networking with real-time impairment awareness," OSA Optics Express, vol. 19, pp. B736-B745, 2011.

[19] Ll. Gifre, A. P. Vela, M. Ruiz, J. López de Vergara, and L. Velasco, "Experimental Assessment of Node and Control Architectures to Support the Observe-Analyze-Act Loop," in Proc. IEEE/OSA Optical Fiber Communication Conference (OFC), 2017.

[20] L. Velasco, Ll. Gifre, J.-L. Izquierdo-Zaragoza, F. Paolucci, A. P. Vela, A. Sgambelluri, M. Ruiz, and F. Cugini, "An Architecture to Support Autonomic Slice Networking [Invited]," IEEE/OSA Journal of Lightwave Technology (JLT), 2017 (DOI: 10.1109/JLT.2017.2748233).

[21] P. Khodashenas, J. Rivas-Moscoso, B. Shariati, D. Marom, D. Klonidis, and I. Tomkos, "Investigation of spectrum granularity for performance optimization of flexible Nyquist-WDM-based optical networks," IEEE/OSA Journal of Lightwave Technology (JLT), vol. 33, pp. 4767–774, 2015.

[22] N. Sambo et al., "Modeling and Distributed Provisioning in 10-40-100 Gb/s Multirate Wavelength Switched Optical Networks," IEEE/OSA Journal of Lightwave Technology, vol. 29, pp. 1248-1257, 2011.

[23] S. R. Safavian and D. Landgrebe, "A survey of decision tree classifier methodology," IEEE Transactions on Systems, Man, and Cybernetics, vol. 21, no. 3, pp. 660-674, 1991.

[24] C. Bishop, *Pattern Recognition and Machine Learning*, Springer-Verlag, 2006.